Macromolecules

Volume 39, Number 5 March 7, 2006

Communications to the Editor

Order versus Disorder: Effect of Structure on the Mechanical Properties of Polymer Material

Daniele Fava,[†] Ying S. Fan,[⊥] Eugenia Kumacheva,*[,†,‡,§] Mitchell A. Winnik,[†,‡] and Douglas M. Shinozaki*[,⊥]

Department of Chemistry, University of Toronto, 80 Saint George Street, Toronto, Ontario M5S 3H6, Canada; Department of Chemical Engineering and Applied Chemistry, University of Toronto, 200 College Street, Toronto, Ontario M5S 3E5, Canada; Institute of Biomaterials and Biomedical Engineering, University of Toronto, 4 Taddle Creek Road, Toronto, Ontario M5S 3H6 Canada; and Department of Mechanical and Materials Engineering, The University of Western Ontario, London, Ontario N6A 5B9, Canada

Received November 17, 2005

Revised Manuscript Received January 6, 2006

Nature provides us with a variety of polymer−inorganic or polymer−polymer composite materials with remarkable mechanical properties. The variables that determine the mechanical properties of these materials can be divided in two categories: compositional and structural. Compositional variables are determined by the mechanical properties of the individual components and the strength of the interactions between these components. The structural variables are governed by the mutual arrangement of the components in the composite material. It is believed that the outstanding mechanical properties of nacre, bones, tendons, or plant tissues are largely governed by the intrinsic structures of these materials.[1−4] For example, the strength and hardness of nacre are attributed to the highly ordered arrangement of hard $CaCO_3$ platelets and elastic organic layers to form a composite material with a "brick and mortar" structure.[1] In the case of bones, a lamellar bone, in which the collagen fibers are aligned parallel to each other, is stronger than woven bone, in which the collagen fibers are distributed randomly.[2] Understanding the role of structure in the variation of mechanical properties is vital in the design of new materials, especially when a biomimetic approach is to be exploited.

In the present work, we used a model system to examine the role of structure in the mechanical properties of composite polymers. We obtained polymer films from latex particles which are known for their ability to self-assemble in three-dimensional arrays with a high degree of order and symmetry.[5−8] Furthermore, we used a "core−shell" approach to polymer nanostructured materials:[9] the films were produced from latex particles comprising a rigid core and a soft shell. A specific relation between the composition of the core-forming polymer (CFP) and the shell-forming polymer (SFP) was such that $T_{g,SFP} < T_{ff} < T_{g,CFP}$, where $T_{g,CFP}$ and $T_{g,SFP}$ are the glass transition temperatures of CFP and SFP, respectively, and T_{ff} is the temperature of film formation. Following a "core−shell" approach, we obtained composite films in which the array of rigid particles (the former latex cores) was embedded into the soft elastomeric matrix of the shell-forming polymer. Strong chemical bonding between the inclusions and the matrix avoided ambiguity in interpreting the results of the experiments on the deformation of the material. The rigid inclusions were organized in a periodic or random fashion, as shown schematically in Figure 1a,b.

A significant number of reports exist on the mechanical properties of composite elastomeric films. Typically, such films are reinforced by embedding inorganic particles (e.g., SiO_2 beads) or organic particles (e.g., high glass transition temperature polymer) into the elastomeric matrix.[10−13] Polymer−polymer composite films were obtained from a mixture of hard and soft latex particles or from the core−shell particles with a hard core and a soft shell.[11,12] The resulting films typically feature random distribution of hard inclusions in the elastic matrix. Three reports deserve particular attention. Lepizzera et al. used atomic force microscopy to study films with a periodic structure obtained

[†] Department of Chemistry, University of Toronto.
[‡] Department of Chemical Engineering and Applied Chemistry, University of Toronto.
[§] Institute of Biomaterials and Biomedical Engineering, University of Toronto.
[⊥] The University of Western Ontario.
* To whom correspondence should be addressed: e-mail ekumache@chem.utoronto.ca.

10.1021/ma052470p CCC: $33.50
Published on Web 02/02/2006

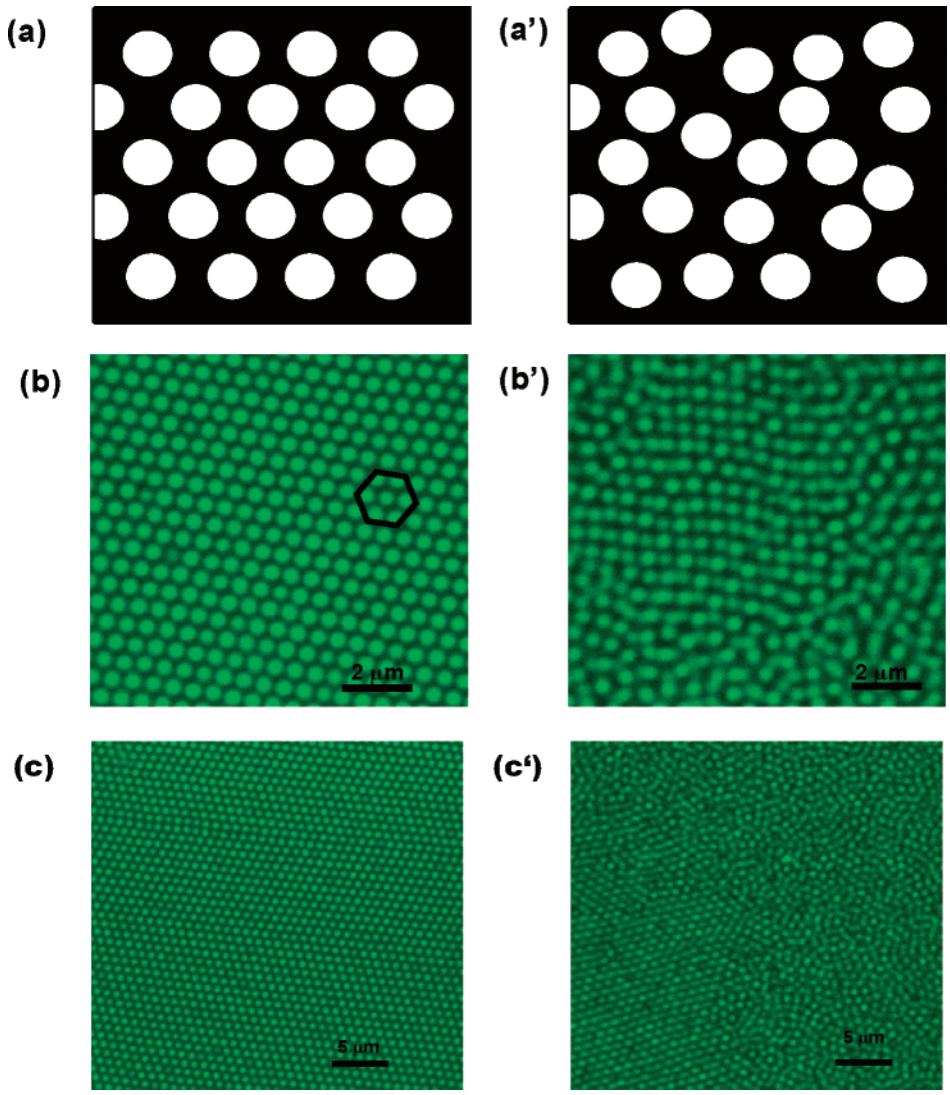

Figure 1. (a, a′) Schematic illustration (top view) of ordered and disordered films, respectively. (b, b′, c, c″) Confocal fluorescence microscopy images of ordered (b, c) and disordered (b′, c′) films. Films were imaged 50 μm (b, b′) and 166 μm (c, c′) below the top surface. Dye-labeled latex cores appear bright on the dark background of the optically inert shell-forming polymer. $\lambda_{exc} = 488$ nm. In b, b′ the scale bar is 2 μm. In c, c′ the space bar is 5 μm.

from core−shell particles with a rigid poly(methyl methacrylate) core and a soft poly(butyl acrylate-*co*-methyl methacrylate-*co*-acrylic acid) shell.[11] In this work, no information about the bulk morphology of the films was provided. In a related article, the same authors provided a model for the deformation mechanism of the films.[13] However, the effect of the distribution of inclusions was not investigated. Mark et al. prepared films in which silica particles were randomly or regularly dispersed in a poly(methyl acrylate) elastomeric matrix.[14] The authors found that the level of material reinforcement was the same for the composite films with a regular arrangement, and with a random arrangement, of silica microspheres.

In the present study, we examined the structure and properties of two types of films with the same composition, but different structure. In both films, hard inclusions were embedded in an elastomeric matrix, yet in the first type of films, these inclusions were randomly distributed in the matrix, whereas in the second type, the inclusions were arranged in an ordered fashion. Later in the text the two systems will be referred to as "disordered" and "ordered" films, respectively.

The films were prepared form core−shell particles comprising a rigid poly(methyl methacrylate-*co*-butyl acrylate) core and a soft poly(methyl methacrylate-*co*-butyl acrylate) shell. Both the CFP and the SFP were cross-linked with 0.8 mol % of ethylene glycol dimethacrylate (EGDMA). The core−shell particles were prepared via surfactant-free emulsion polymerization, as described in the Supporting Information. The weight ratios poly(methyl methacrylate)/poly(butyl acrylate) in the CFP and SFP were 9/1 and 0.8/1, respectively, which yielded glass transition temperatures of ca. 130 and 12 °C, respectively. The CFP was covalently labeled with a fluorescent dye (NBD, $\lambda_{ab} = 470$ nm, $\lambda_{em} = 505-550$ nm) using the methacrylate derivative of NBD that we have reported in our previous publications.[9] Thus, we were able to use laser confocal fluorescence microscopy (LCFM) to image the surface and the bulk distribution of the rigid inclusions of CFP in the composite films.

Ordered films were prepared by allowing core−shell particles to settle over ca. 2 weeks in a Teflon Petri dish covered with a watch glass. After 2 weeks the watch glass was removedto allow water evaporation and film formation at room temperature. Disordered films were prepared by adding a few drops of methanol to the latex dispersion and allowing for water evaporation overnight. The thickness of films was varied from 0.5 to 1.0 mm.

Parts b and b′ of Figure 1′ show the LCFM images of the ordered and disordered films, respectively, acquired 50 μm

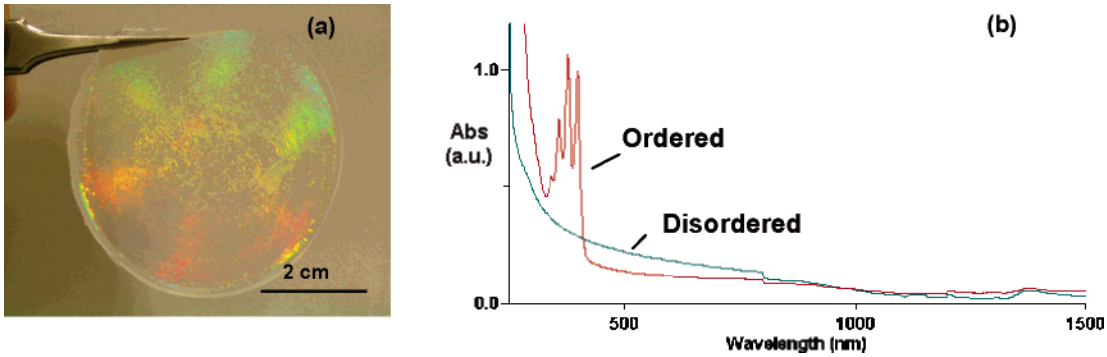

Figure 2. (a) Photograph of an ordered film showing iridescence. (b) UV−vis spectrum of ordered and disordered samples. The peaks for the ordered films are centered at 358, 377, and 398 nm.

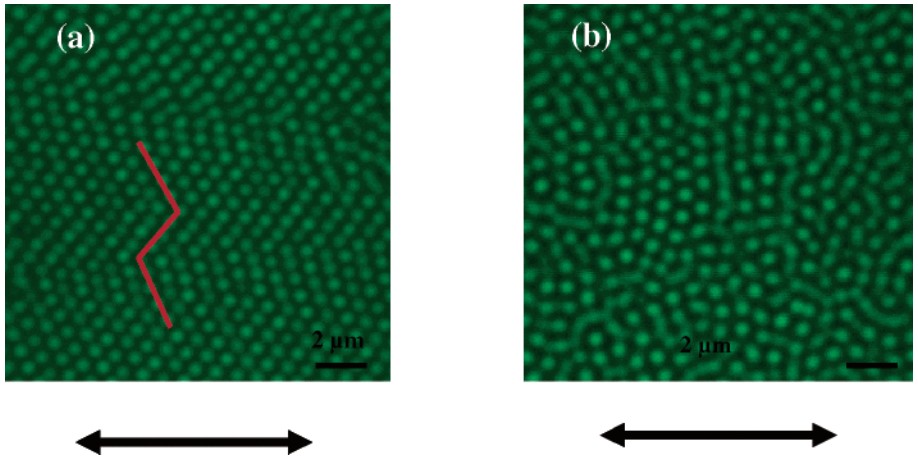

Figure 3. (a) Typical LCFM images of ordered (a) and disordered (b) films stretched to ca. 140% of the original dimensions. The images are acquired at the distance 50 μm from the top surface. Film elongation was in the direction indicated by the double arrows beneath the images.

below the film surface. The fluorescent inclusions of rigid CFP appear bright on the dark background of the nonfluorescent SFP. In both films the volume fraction of the 600 nm size fluorescent core particles was ca. 30%. In Figure 1b an ordered film shows a substantial long range order in the $x-y$ plane corresponding to fcc packing in the bulk of the film, along with occasional grain boundaries observed under low magnification in Figure 1c. These defects did not tend to feature any preferential alignment in the composite films. The disordered films showed no periodic organization of the inclusions anywhere in the sample. The difference in the morphology of the ordered and disordered films in Figure 1 was drastic and sufficiently large to extract the role of structure in the mechanical properties of the material. The arrangement of microspheres was preserved in the z-direction, as shown in Figure 1c,c′ for the plane localized at 166 μm below the top surface.

The ordered films featured iridescence in the transmission mode, as shown in Figure 2a. We stress that iridescence occurred at a very small refractive index difference between the matrix and the particles: on the basis of the composition of the CFP and SFP in the core−shell particles, we estimate the refractive index contrast to be ca. 0.01. To verify whether iridescence was owing to the entrapment of air bubbles in the films and/or to the periodic surface roughness of the films,[9] we conducted two control experiments. First, we prepared ordered films in a vacuum oven (still following the protocol of film preparation described above). Qualitatively, the resulting films showed iridescence similar to that of the films prepared in air. Second, we reduced the surface roughness of the ordered films by pressing them for about 5 min against Teflon-covered metal slides in a Carver press at 30 °C (that is, ca. 20 °C above the T_g of the SFP) at a pressure of 1 ton/m^2. Following this procedure, both the top and the bottom surface of the films became smooth; nevertheless, iridescence was preserved.

Figure 2b shows the UV−vis spectra of the ordered and disordered films measured in the range 250−1500 nm. For the ordered films no diffraction peak was detected in the spectral region 900−1100 nm of the spectrum, as it would have been expected from the lattice constant. We observed, however, three distinct sharp peaks centered at 358, 377, and 398 nm, whereas for the disordered sample, no peaks appeared in the entire spectral range studied (Figure 2b). The origin of the peaks for the ordered films is currently under investigation; we believe, however, that the peaks measured are due to high-order diffraction.[15]

The morphology of ordered and disordered films showed different response to deformation. Figure 3 shows the structure of films elongated to ca. 140% of their original length as imaged with LCFM. In the stretched ordered films (Figure 3a), the rigid fluorescent particles rearranged to form zigzag rows with the long axis oriented perpendicular to the direction of the elongation. Similar rearrangement of the inclusions on the surface of similar films has been previously reported by Lepizzera et al.,[11] who explained the formation of the zigzag patterns in the following way. In the initial stage of elongation, the particles are pushed together in the direction perpendicular to elongation, resulting in the formation of rows oriented perpendicularly to the direction of stretching. As the elongation increased, the particles were pulled apart in the direction of the elongation giving rise to the zigzag patterns.[11] We note that that visually the zigzag features seen in Figure 3a resemble the grain boundaries in the nondeformed films seen in Figure 1c; however, in contrast with lattice defects, the chevrons seen in Figure 3a have a smaller characteristic length and a preferential alignment

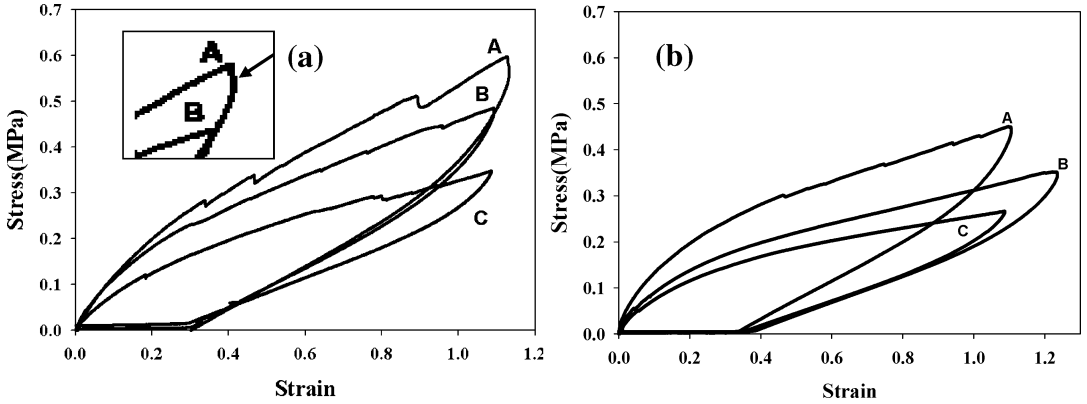

Figure 4. Stress−strain curves of (a) disordered and (b) ordered films. Strain rates: 1.35×10^{-3} s^{-1} (A), 1.08×10^{-3} s^{-1} (B), and 0.27×10^{-3} s^{-1} (C). In (a) the inset provides an expanded view of the initial stage of the unloading curve A.

with respect to the direction of deformation. The system with a random distribution of the rigid inclusions showed no geometrical rearrangement of the core particles upon elongation (Figure 3b).

We compared the mechanical properties of the two types of films by performing stress−strain and indentation tests. Parts a and b of Figure 4 show the results of stress−strain experiments acquired at different strain rates for the ordered and disordered samples, respectively. In Figure 4a, the stress−strain curves of the disordered material show lower stresses at slow deformation rate (curves B and C) than the stresses measured at higher strain rates (curve A), as expected for viscoelastic materials.[16] The unloading curves showed ca. 70% strain recovery on the time scale of the measurement, followed by a much slower recovery to almost zero residual strain, in accordance with the time-dependent behavior of elastic matrices.[17] For the stress−strain curves acquired at the highest strain rate, a slight increase in strain was observed in the initial stage of the unloading (curve A and inset, Figure 4a), probably due to a time-dependent creep in the elastomeric phase.[18] Small stress drops were measured in loading curves as the toothlike indentations. This trend was more pronounced for higher deformation rates.

The overall appearance of the stress−strain curves acquired for the disordered films was similar to that of the ordered films (Figure 4b). Two features deserve special attention. First, for the strain rates used in the present study, the films with ordered morphologies showed 25−30% lower stress than the disordered films; i.e., the ordered films were softer than the films with a disordered structure. Furthermore, stress drops measured for the loading curves were noticeably smaller than for the disordered films.

We explain the results of strain−stress experiments as follows. For fcc crystals, the octahedral (111) planes have the highest interplanar distance. In a composite material subjected to stress, progressive deformation occurs by shear in the (111) planes. In the disordered film, randomly distributed hard particles obstruct shear in these planes until the stress becomes sufficiently high to overcome the barriers. By contrast, in the ordered film shear occurs with no obstructions, which results in lower stresses developed in such films.

The phenomenon of the periodic increase and reduction in stress shown as serrations in the stress−strain curve (Figure 4a,b) originates from a slip in the soft matrix in the (1,1,1) plane, which causes the stored strain energy to be released. The greater prominence of this effect in the disordered films, as well as for the high stress rates for both types of films, is due to the higher stresses available. We speculate that the slip occurs due to the disentanglement and pullout of dangling ends in the SFP.

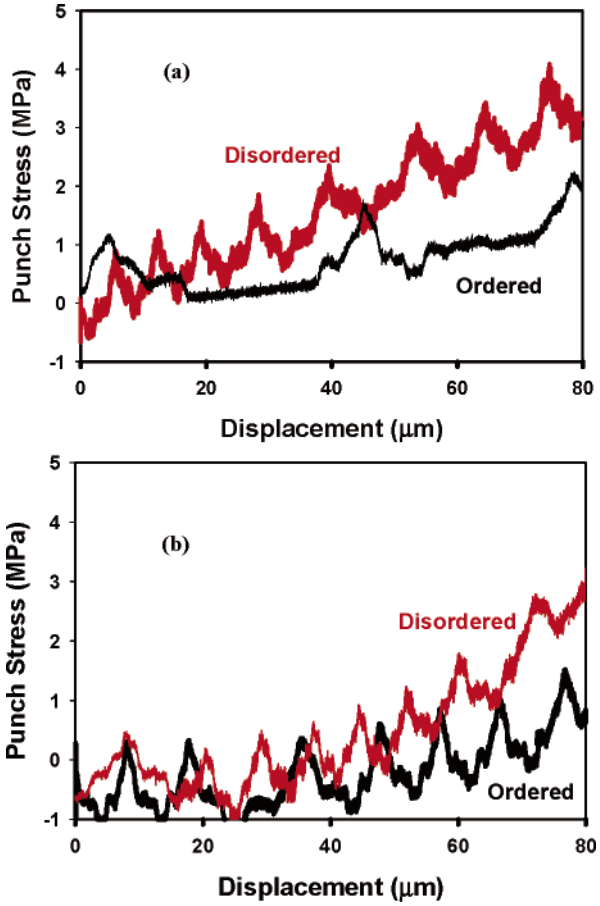

Figure 5. Indentation curves of ordered and disordered samples acquired in loading (a) and unloading (b) experiments. The loading rate and the maximum depth of penetration were 0.22 μm/s and 80 μm, respectively.

Slippage in the elastomeric matrix was confirmed in the microindentation tests (Figure 5). The deep penetration tests were carried out on ca. 500 μm thick films using a 80 μm diameter cylindrical indenter described in detail elsewhere.[19]

Analysis of the stress−strain fields under the tip during penetration showed that the shapes of the curves can be related directly to the elastic and viscoelastic properties of the material under study. Figure 5 shows that the ordered material was softer than the disordered one, consistent with the tensile tests described above. Upon loading, the large serrations in the load−displacement curves were distinct for the two types of polymer films; however, for the disordered material they were more closely spaced on the displacement axis. This observation is

consistent with the suggestion from the tensile tests that slip blockage and release of stress were responsible for the serrations. The effect was similar to the serrated load−displacement curves acquired in the nanoindentation of amorphous metals,[20] although the strain-rate dependence was different than in the polymer composite films studied in the present work. For microindentation of isotropic solids, the major slip occurs in planes oblique to the penetration axis. In the disordered material, as explained for stress−strain measurements, the randomly distributed inclusions prevented the planes from slipping. The barrier is overcome at high applied stress, and a sudden slip of planes takes place (which results in the serrations in the indentation plots). In the disordered film, the irregular placement of hard particles results in blockage and release of the planes at small displacement intervals. The smaller number of randomly distributed inclusions in the ordered material resulted in a less frequent blockage and release of the planes. We would like to point out an important difference between the loading and unloading curves for the ordered sample: the loading curve showed a significantly smaller number of serrations than the unloading curve. The unloading curves of the ordered and disordered films were quite similar probably due to the less organized structure of the ordered films after deformation.

In summary, we showed that polymer composite films with random and periodic structures show a different response to deformation. Following elongation, films with ordered morphologies undergo structural rearrangement: hard inclusions align to form long zigzag rows. By contrast, such rearrangement was not observed in the films with a random distribution of rigid inclusions. The disordered films were 25−30% harder than the ordered films. We believe that the difference originates from the intrinsic structure of the two films: in the disordered films, shear in (111) planes of the elastomeric matrix is blocked by the randomly distributed rigid inclusions while in the ordered samples shear is essentially not suppressed. The disordered material was prone to the slip, causing the stored energy to be released. These findings are important for the design of new materials with optimized mechanical properties.

Acknowledgment. The authors thank NSERC Canada and the Province of Ontario under their ORDCF program for their support of this work. The authors are grateful to Dr. Pakula (Max Planck Institute for the Polymer Research) for the measurements of polymer glass transition temperatures by differential scanning calorimetry and dynamic mechanical analysis. and to Prof. Fratzl for useful discussions. E.K. acknowledges funding under the Canada Research Chair Program.

Supporting Information Available: Preparation of core−shell particles via surfactant-free emulsion polymerization. This material is available free of charge via the Internet at http://pubs.acs.org.

References and Notes

(1) Smith, B. L.; et al. *Nature (London)* **1999**, *399*, 762−763.
(2) Martin, R. B. *J. Biomech.* **1991**, *24* (Suppl. 1), 79−88.
(3) Thompson, J. B.; Kindt, J. H.; Drake, B.; Hansma, H. B.; Morse, D. E.; Hansma, P. K. *Nature (London)* **2001**, *414*, 773−776.
(4) Fratzl, P.; Gupta, H. S.; Paschalis, E. P.; Roschger, P. J. *J. Mater. Chem.* **2004**, *14*, 2115−2123.
(5) Davis, K. E.; Russel, W. B.; Glantschnig, W. *J. Chem. Soc., Faraday Trans.* **1991**, *87*, 411−424.
(6) Holland, B. T.; Blanford, C. F.; Stein, A. *Science* **1998**, *281*, 538−540.
(7) Jiang, P.; Bertone, J. F.; Hwang, K. S.; Colvin, V. L. *Chem. Mater.* **1999**, *11*, 2132−2140.
(8) (a) Vickreva, O.; Kalinina, O.; Kumacheva, E. *Adv. Mater.* **2000**, *12*, 110−112. (b) Allard, M.; Sargent, E. H.; Kumacheva, E.; Kalinina, O. *J. Opt. Quantum Electron.* **2002**, *34*, 27−36.
(9) (a) Kalinina, O.; Kumacheva, E. *Macromolecules* **1999**, *32*, 4122−4129. (b) Kalinina, O.; Kumacheva, E.; Lilge, L. *Adv. Mater.* **1999**, *11*, 231−234.
(10) Mullins, L.; Tobin, N. R. *J. Appl. Polym. Sci.* **1965**, *9*, 2993−3009.
(11) Lepizzera, S.; Sheer, M.; Fond, C.; Pith, T.; Lambla, M.; Lang, J. *Macromolecules* **1997**, *30*, 7953−7957.
(12) Lepizzera, S.; Lhommeau, C.; Dilger, G.; Pith, T.; Lambla, M. *J. Polym. Sci., Part B: Polym. Phys.* **1997**, *35*, 2093−2101.
(13) Lepizzera, S.; Pith, T.; Fond, C.; Lambla, M. *Macromolecules* **1997**, *30*, 7945−7952.
(14) Mark, J. E.; Pu, Z.; Jethmalany, J. M.; Ford, W. T. *Chem. Mater.* **1997**, *9*, 2442−2447.
(15) Asher, S.; Weismann, J. M.; Tikhonov, A.; Coalson, R. D.; Kesavamoorthy, R. *Phys. Rev. E* **2004**, *69*, 066619/1−066619/14.
(16) McCrum, N. G.; Buckley, C. P.; Bucknall, C. B. *Principles of Polymer Engineering*; Oxford Science Publication, Oxford, UK, 1997.
(17) Gent, A. N. *Engineering with Rubber*; Hanser Gardner Publisher: Munich, Germany, 2001.
(18) When the unloading begins, the strain increases as the stress decreases because the strain rate applied by the instrument is slower than the forward creep rate of the sample at that applied stress.
(19) Lu, Y.; Shinozaki, D. M. *J. Mater. Sci.* **2002**, *37*, 1283−1293.
(20) Wei, B. C.; Zhang, T. H.; Li, W. H.; Sun, Y. F.; Yu, Y.; Wang, Y. R. *Intermetallics* **2004**, *12*, 1239−1243.

MA052470P